nature physics

ARTICLES

PUBLISHED ONLINE: 27 FEBRUARY 2017 | DOI: 10.1038/NPHYS4051

# Orthogonal magnetization and symmetry breaking in pyrochlore iridate $Eu_2Ir_2O_7$

Tian Liang[1*†‡], Timothy H. Hsieh[2†‡], Jun J. Ishikawa[3], Satoru Nakatsuji[3,4], Liang Fu[2] and N. P. Ong[1*]

**Electrons in the pyrochlore iridates experience a large interaction energy in addition to a strong spin–orbit interaction. Both features make the iridates promising for realizing novel states such as the topological Mott insulator. The pyrochlore iridate $Eu_2Ir_2O_7$ shows a metal–insulator transition at $T_N \sim 120$ K below which a magnetically ordered state develops. Using torque magnetometry, we uncover an unusual magnetic response. A magnetic field $H$ applied in its $a$–$b$ plane produces a nonlinear magnetization $M_\perp$ orthogonal to the plane. $M_\perp$ displays a $d$-wave field-angle pattern consistent with octupolar order, with a handedness dictated by field cooling, leading to symmetry breaking of the chirality $\omega$. A surprise is that the lobe orientation of the $d$-wave pattern is sensitive to the direction of the field when the sample is field-cooled below $T_N$, suggestive of an additional order parameter $\eta$ already present at 300 K.**

The pyrochlore iridates, comprised of networks of vertex-sharing tetrahedra[1,2], have emerged as candidates for investigating the role of interactions in topological matter[1,3]. The phase diagram is predicted to have topological states with exotic excitations[4–8]. At each $Ir^{4+}$ site, the five $5d$ electrons occupy the six $t_{2g}$ orbitals derived from $d_{xy}$, $d_{yz}$ and $d_{zx}$ states (crystal field splitting lifts the $e_g$ orbitals high above the $t_{2g}$ manifold). The large spin–orbit interaction (SOI) splits the $t_{2g}$ manifold into a $J = 1/2$ doublet with energy $\lambda$ and a $J = 3/2$ quadruplet with energy $-\lambda/2$ (refs 3,9,10). At the critical temperature $T_N \sim 120$ K, $Eu_2Ir_2O_7$ undergoes a transition to an insulating state (Fig. 1a)[11–14] where a magnetically ordered state emerges[15–22].

In a magnetically ordered state, the free energy $F$ and the magnetization $\mathbf{M}$ of a system can be expanded, up to third order, as follows:

$$F = -\mathbf{M}^{\mathrm{d}} \cdot \mathbf{H} - \chi^{\mathrm{p}}_{ij} H_i H_j - Q_{ij} H_i H_j - \omega_{ijk} H_i H_j H_k \quad (1)$$

$$M_i = -\partial F/\partial H_i = M^{\mathrm{d}}_i + \chi^{\mathrm{p}}_{ij} H_j + Q_{ij} H_j + \omega_{ijk} H_j H_k \quad (2)$$

Here $\mathbf{M}^{\mathrm{d}}$ (vector) is the conventional dipolar order, $Q_{ij}$ (second rank tensor) is the quadrupolar order, $\omega_{ijk}$ (third rank tensor) is the octupolar order, and $\chi_{ij}$ is the conventional paramagnetic susceptibility, with $i, j, k$ referring to components along the unit cell vectors $\mathbf{a}$, $\mathbf{b}$, $\mathbf{c}$. $\mathbf{M}^{\mathrm{d}}$, $Q_{ij}$, $\omega_{ijk}$ represent independent order parameters respectively. We note that, whereas $\mathbf{M}^{\mathrm{d}}$, $Q_{ij}$, $\omega_{ijk}$ all change their sign under inversion or time reversal (for example, inverting the field-cooling direction), $\chi_{ij}$ (the paramagnetic susceptibility describing the Zeeman effect) is unaffected by these operations. Specifically, under time reversal, the magnetization $\mathbf{M}$ of the system becomes

$$M_i = -M^{\mathrm{d}}_i + \chi^{\mathrm{p}}_{ij} H_j - Q_{ij} H_j - \omega_{ijk} H_j H_k \quad (3)$$

Comparison between equations (2) and (3) shows that $\chi_{ij}$ transforms differently from $Q_{ij}$ (as well as $\mathbf{M}^{\mathrm{d}}$ and $\omega_{ijk}$). We also note that for systems with inversion symmetry, such as $Eu_2Ir_2O_7$, the quadrupolar term $Q_{ij}$ vanishes ($F \to F$, $Q_{ij} \to -Q_{ij}$, $H \to -H$). Therefore, the free energy $F$ and magnetization $\mathbf{M}$ for $Eu_2Ir_2O_7$ can be written as

$$F = -\mathbf{M}^{\mathrm{d}} \cdot \mathbf{H} - \chi^{\mathrm{p}}_{ij} H_i H_j - \omega_{ijk} H_i H_j H_k \quad (4)$$

$$M_i = M^{\mathrm{d}}_i + \chi^{\mathrm{p}}_{ij} H_j + \omega_{ijk} H_j H_k \equiv M^{\mathrm{d}}_i + M_{\mathrm{p}} + M_\perp \quad (5)$$

The third term of equation (5), $M_\perp = \omega_{ijk} H_j H_k$, which we call orthogonal magnetization, directly detects the octupolar order $\omega_{ijk}$. We note that for a conventional antiferromagnet/ferromagnet, only the first two terms of equation (5) exist and the third term $\omega_{ijk}$ is absent. Therefore, the detection of the orthogonal magnetization $M_\perp = \omega_{ijk} H_j H_k$ is direct evidence for the 'hidden order' of the system.

Although the magnetization described by equation (5) is very interesting, no experiment has been reported. In our experiments, a field $\mathbf{H} = (H_a, H_b, 0)$ confined to the $a$–$b$ plane produces a nonlinear magnetization $\mathbf{M}_\perp$ normal to the plane. Depending on the field-cooling direction, the observed orthogonal magnetization takes the following forms

$$M_\perp = \omega \chi^{y_{\mathrm{fc}}}_\perp H_a H_b \quad (\pm y\text{-axis field cooling}) \quad (6)$$

$$M_\perp = \omega \chi^{x_{\mathrm{fc}}}_\perp H_x H_y \quad (\pm x\text{-axis field cooling}) \quad (7)$$

where the susceptibility $\chi_\perp(T)$ describes its $T$ dependence (an additional phenomenological term $\eta$ is discussed below). In our set-up, we define the (lab) $x$ and $y$ axes as rotated by 45° relative to the lattice vectors $\mathbf{a}$ and $\mathbf{b}$ of the pyrochlore unit cell [$\hat{\mathbf{x}} \parallel [1\bar{1}0]$, $\hat{\mathbf{y}} \parallel [110]$ and $\hat{\mathbf{z}} \parallel [001]$] (Fig. 1b). We emphasize that the direction of $\mathbf{M}_\perp$ cannot be inferred a priori from the signs of $H_a$ ($H_x$) and $H_b$ ($H_y$). By necessity, its appearance spontaneously breaks a $Z_2$ symmetry (the system spontaneously chooses $\omega$ to be either $+1$ or $-1$).

We contrast our case with the trivial case of $Gd_2Ti_2O_7$ (with $T_N \sim 1$ K) in which the applied magnetic field distorts the spin

[1]Department of Physics, Princeton University, Princeton, New Jersey 08544, USA. [2]Department of Physics, Massachusetts Institute of Technology, Cambridge, Massachusetts 02139, USA. [3]Institute for Solid State Physics, University of Tokyo, Kashiwa 277-8581, Japan. [4]CREST, Japan Science and Technology Agency (JST), 4-1-8 Honcho Kawaguchi, Saitama 332-0012, Japan. †Present addresses: Department of Applied Physics, Stanford University, Stanford, California 94305, USA (T.L.); Kavli Institute for Theoretical Physics, University of California, Santa Barbara, California 93106, USA (T.H.H.). ‡These authors contributed equally to this work. *e-mail: liang16@stanford.edu; npo@princeton.edu

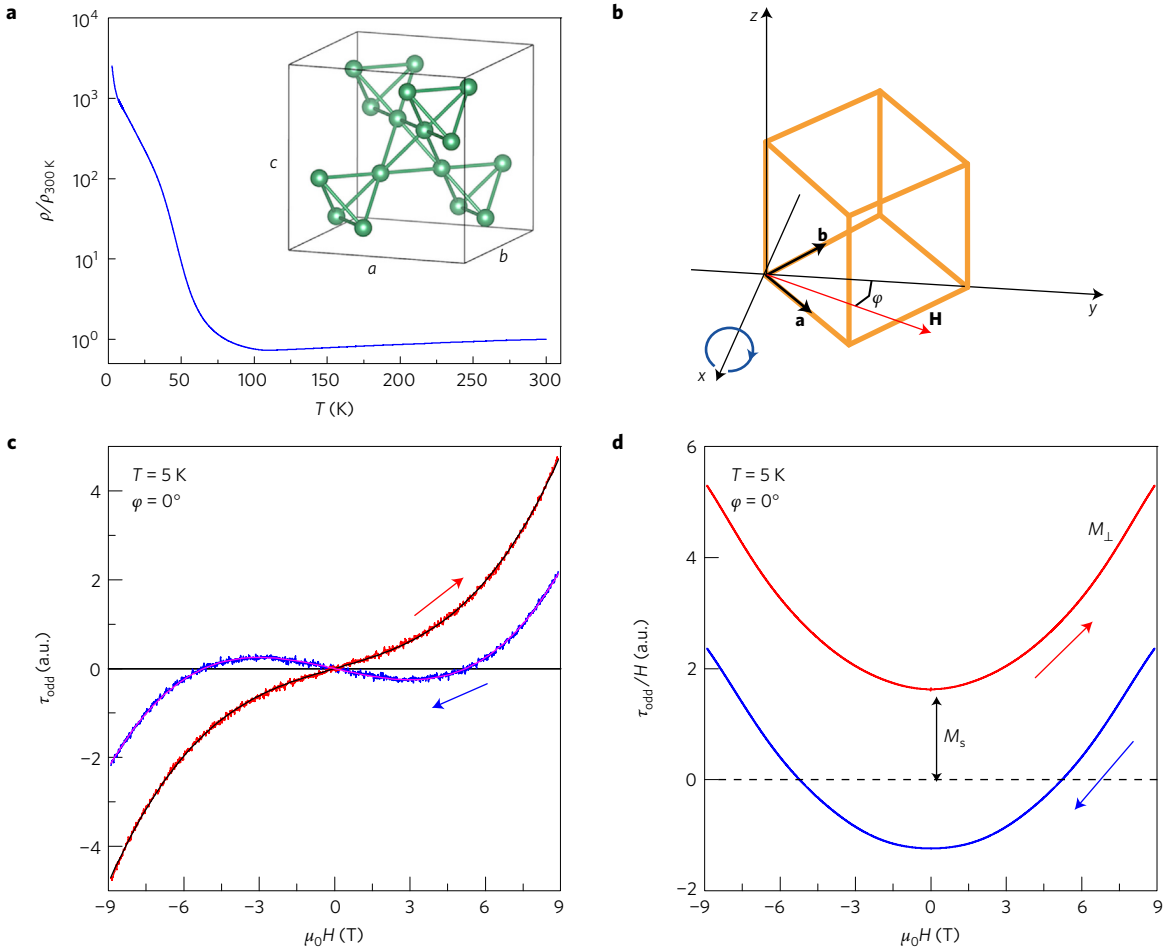


**Figure 1 | Pyrochlore lattice, orientation of the lab axes, and analysis of the torque signal. a**, Lattice of the pyrochlore $Eu_2Ir_2O_7$. **b**, Sketch of the orientation of the lab frame $\hat{\mathbf{x}}$, $\hat{\mathbf{y}}$ and $\hat{\mathbf{z}}$ relative to the lattice vectors **a**, **b** and **c**. The axis of the torque cantilever is parallel to $\hat{\mathbf{x}}$, as indicated by the blue circle. With **H** (red arrow) in the *a*–*b* plane at an angle $\varphi$ to $\hat{\mathbf{y}}$, the torque component detected is $\tau_x = M_z H \cos\varphi$. **c**, Plots of the *H*-odd component of the torque $\tau_{odd}$ measured in field sweep-up (−9 → 9 T, red) and sweep-down (9 → −9 T, blue) scans at 5 K and angle $\varphi = 0°$. **d**, Plot of $\tau_{odd}/H$, which is the sum of the orthogonal magnetization $M_\perp$ (parabolic curve) displaced vertically by a constant term $M_s$. The sign sgn($M_s$) changes with sweep direction. By contrast, sgn($M_\perp$), which identifies $\omega$, is frozen (the parabolae point 'up' in both sweeps); see text for details.

configuration to induce a conventional dipolar magnetization $\mathbf{M}^d = \mathbf{M}_{trans}$, previously called 'transverse' magnetization in refs 23, 24. $\mathbf{M}_{trans}$ does not involve breaking of a $Z_2$ symmetry, but comes just from the conventional Zeeman coupling term $-\mathbf{M}^d \cdot \mathbf{H}$. Crucially, the suppression of this Zeeman-induced coupling in $Eu_2Ir_2O_7$ via large exchange energy $J_{eff} \gtrsim T_N \sim 120$ K allows the octupolar response $M_\perp = \omega_{ijk} H_j H_k$ to emerge. See Methods for more discussion.

We now discuss the experimental data of torque magnetometry. The axis of the torque cantilever is aligned parallel to $\hat{\mathbf{x}}$. With **H** in the *a*–*b* plane (at an angle $\varphi$ to $\hat{\mathbf{y}}$), the torque signal is given by $\tau = M_z H_y$; the torque detects the magnetization component $M_z$ normal to the plane in which **H** lies (Supplementary Figs 2 and 3).

In $Eu_2Ir_2O_7$, $M_z$ consists of three terms $M_s \propto H^0$, $M_p \propto H$, $M_\perp \propto H^2$: namely, $M_z = M_s + M_p + M_\perp$. Accordingly, the observed torque (with $\varphi$ and $T$ fixed) can be represented as

$$\tau \equiv \tau_s + \tau_p + \tau_\perp = \alpha H + \beta H^2 + \gamma H^3 \qquad (8)$$

(We refer to the *H*-even and *H*-odd parts as $\tau_{even} \equiv \tau_p = \beta H^2$ and $\tau_{odd} \equiv \tau_s + \tau_\perp = \alpha H + \gamma H^3$, respectively.) The first term $\alpha H$ corresponds to a field-independent magnetization $M_s \equiv \alpha/\cos\varphi$. The second term $\tau_{even}$—the largest term in our field range—comes from a paramagnetic magnetization $M_p \equiv \beta H/\cos\varphi$. In contrast to $M_s$ and $M_p$, which persist up to 300 K, the third term $\gamma H^3$, which onsets below $T_N = 120$ K, corresponds to the orthogonal magnetization $M_\perp \equiv \gamma H^2/\cos\varphi$ arising from the octupolar order.

By antisymmetrization, we can isolate $\tau_{odd}$, which we plot in Fig. 1c at 5 K. The plot clearly shows the $H^3$ variation produced by $M_\perp$ (plus a term from $M_s$). Dividing by $H$, we then isolate $M_\perp$ as a parabola displaced vertically by a constant term $M_s$ (Fig. 1d). We note that the sign of the constant, sgn($M_s$), reverses between sweep-up and -down curves as expected. However, sgn($M_\perp$) and its absolute value (namely, the curvature of the parabola) stay the same, implying completely different origins between $M_\perp$ and $M_s$ (as well as $M_p$). The contrast sharply excludes the possibility that the orthogonal magnetization $M_\perp$ comes from contamination by the dipolar term $\mathbf{M}^d$. If $M_\perp$ came from the dipolar term $\mathbf{M}^d$, it would have shared the same hysteresis patterns of $M_s$. Below, we identify $M_s$ to be related to the phenomenological $\eta$ term which is already present at 300 K. The striking rigidity of sgn($M_\perp$) implies an unusual domain-wall feature of the octupolar order. The procedure is repeated over selected angles $0 < \varphi < 360°$ to isolate the $T$ dependence of $M_\perp$ from 5 K to 300 K.

First, we examine the angular variation of $M_\perp$ at 5 K. As shown in Fig. 2a, the curve of $\tau_\perp = M_\perp H \cos\varphi$ versus $\varphi$ is plotted. The angular

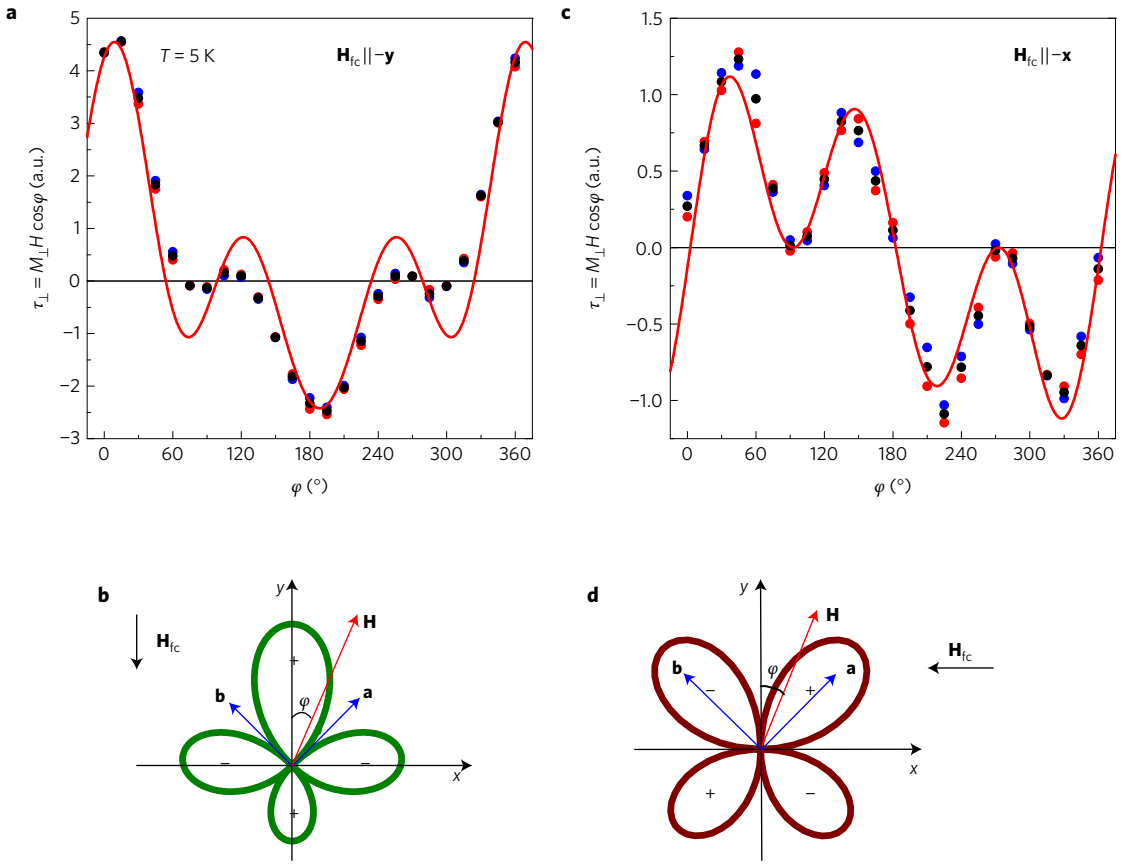


**Figure 2 | Angular variation of $\tau_\perp \equiv M_\perp H\cos\varphi$ and the effect of $H_{fc}$ on the *d*-wave orientation of $M_\perp$.** **a**, $\tau_\perp$ versus $\varphi$ obtained after cooling in $\mathbf{H}_{fc} \parallel -\hat{\mathbf{y}}$. The red curve is the expression $M_\perp \cos\varphi \sim (1+\eta\cos\varphi)\cos 2\varphi \cdot \cos\varphi$, which fits the data well except near 90° and 270°. **b**, Curve describing the skewed *d*-wave pattern with lobes directed along the *x* and *y* axes. The signs of the lobes are reversed if the sample is cooled with $\mathbf{H}_{fc}$ reversed in sign ($\parallel \hat{\mathbf{y}}$). **c**, The experiment is next repeated with $\mathbf{H}_{fc}$ rotated to $\parallel -\hat{\mathbf{x}}$. As shown, the angular variation of $\tau_\perp$ is now different from **a**. The data fit well to the expression $(1+\eta\cos\varphi)\sin 2\varphi \cdot \cos\varphi$. **d**, Polar representation shows a *d*-wave pattern rotated relative to **b**, with lobes now directed along the *a* and *b* axes. The signs of the lobes are reversed if $\mathbf{H}_{fc}$ is reversed in sign. In **a** and **c**, red (blue) symbols are data obtained in sweep-up (sweep-down) scans, while black symbols indicate their average.

variation is nominally described by the red curve representing a *d*-wave form $\cos 2\varphi$ (panel b), viz.

$$M_\perp(T,\varphi) = \chi_\perp(T)H^2(1+\eta\cos\varphi)\cos 2\varphi \qquad (9)$$

where the 'orthogonal' susceptibility $\chi_\perp(T)$ grows like an order parameter below $T_N$. The parameter $\eta$, which distorts the *d*-wave pattern, is a phenomenological term that represents an additional order that already exists at 300 K (see below and section D of Methods). The results in Fig. 2a were measured after field cooling in the (9 T) field $\mathbf{H}_{fc} \parallel -\hat{\mathbf{y}}$. We find that $M_\perp$ changes in sign if $\mathbf{H}_{fc}$ is inverted. We identify the chirality $\omega = 1$ if $\mathbf{H}_{fc} \parallel -\hat{\mathbf{y}}$ (and $-1$ if $\mathbf{H}_{fc} \parallel \hat{\mathbf{y}}$). This symmetry breaking of the chirality sharply distinguishes the octupolar nature of $M_\perp$ from 'transverse' magnetization $\mathbf{M}^d = \mathbf{M}_{trans}$ whose origin is strictly dipolar.

Further evidence for the octupolar origin of $M_\perp$ derives from the hysteretic behaviour of the domain walls (DWs) versus $T$. In conventional dipolar magnets, $\mathbf{H}$ exerts a strong force on the DW because of dipolar coupling. By contrast, for the DW between octupolar domains, a much weaker force is expected. We next describe evidence that the DWs for $M_\perp$ are virtually immobile at low $T$. As already noted in Fig. 1d, $\mathrm{sgn}(M_\perp)$ is 'frozen', unlike $\mathrm{sgn}(M_s)$. As $T$ is raised above 25 K, the reversibility gives way to a large hysteresis. At 60 K, $\tau_\perp$ is strongly hysteretic (Fig. 3a and b show the hysteresis observed for the two *d*-wave patterns attained with different $\mathbf{H}_{fc}$). In Fig. 3c and d, we plot the $T$ dependence of $M_\perp$ measured in up-sweep (red circles) and down-sweep traces (blue) from 5 K to 150 K with $\varphi$ fixed at the lobe maxima.

A striking pattern is that the difference between the red and blue curves (the 'hysteresis amplitude' $\Delta M_\perp$) is largest near 75 K, but rapidly decreases to below resolution for $T < 25$ K. This decrease fits well to the thermal activation form $e^{-\Delta/T}$ with $\Delta = 170$ and 220 K in panels c and d, respectively (Supplementary Fig. 6). At each $T$, $\Delta M_\perp$ measures the distance of DW diffusion on our timescales (sweep rates of 1 T min$^{-1}$). Hence the activated form implies diffusion times that grow exponentially with decreasing $T$. The activated form explains why $\mathrm{sgn}(M_\perp)$ is frozen at 5 K in Fig. 1d. Once a domain pattern is established at 5 K, it is very difficult to erase the pattern because the DWs are immobile on experimental timescales. Both the activated form and the frozen configuration at 5 K reflect the weak coupling of octupolar DWs to $\mathbf{H}$. By contrast, the field-independent term $M_s$ has a very different hysteretic behaviour versus $T$ (Supplementary Fig. 4).

An unexpected finding is that the angular orientation of the *d*-wave lobes can be rotated by cooling in a field $\mathbf{H}_{fc}$ parallel to $-\hat{\mathbf{x}}$, breaking the underlying lattice symmetry between two 'equivalent' axes *x*-axis and *y*-axis (the system is cubic). Cooling to 5 K in the new $\mathbf{H}_{fc}$ leads to the plot of $M_\perp$ shown in Fig. 2c. The *d*-wave pattern (with $\omega = 1$) is now shifted by 45° (Fig. 2d) and described by

$$M_\perp(T,\varphi) = \chi_\perp(T)H^2(1+\eta\cos\varphi)\sin 2\varphi \qquad (10)$$

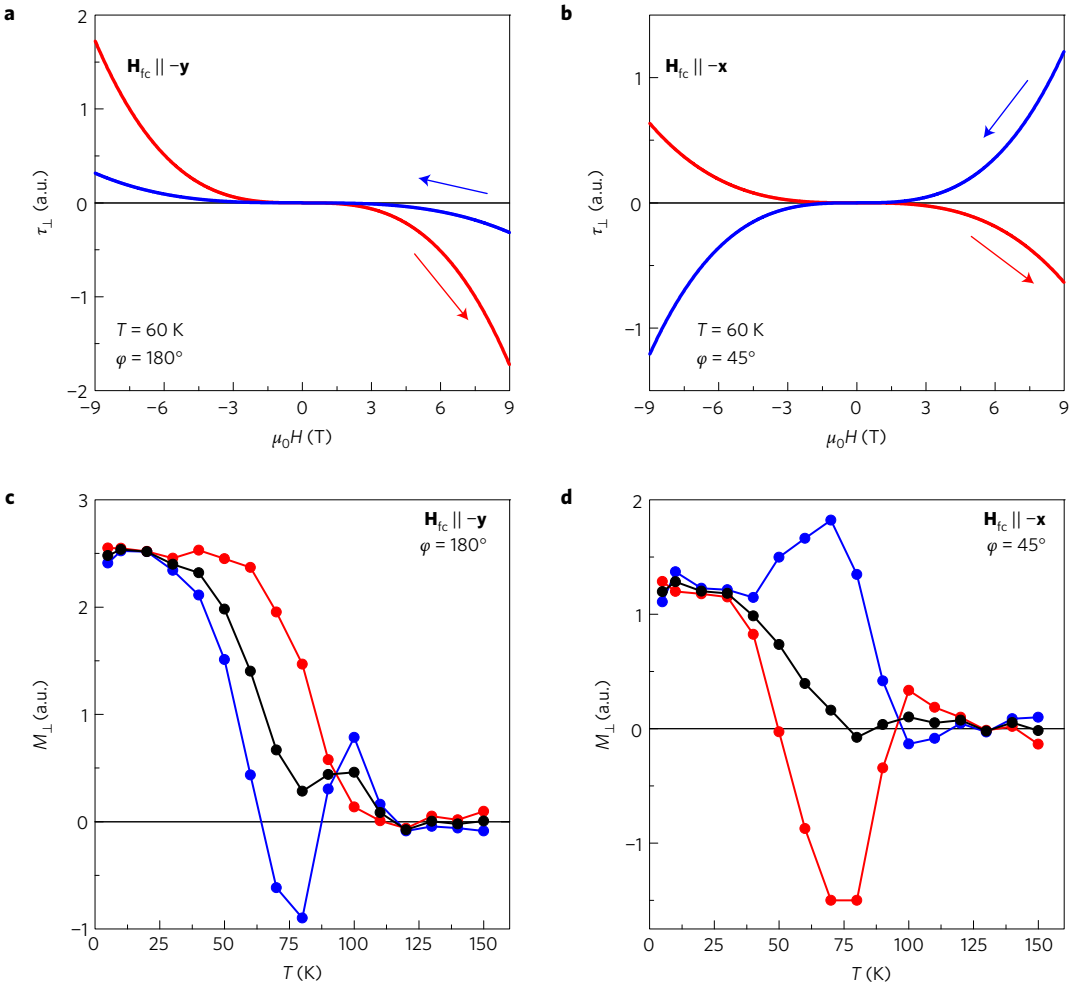


**Figure 3 | Hysteretic behaviour and *T* dependence of the orthogonal magnetization $M_\perp$. a**, Curves of $\tau_\perp$ measured versus $H$ at $T = 60$ K with $\varphi$ fixed at 180° (lobe direction), after cooling in $\mathbf{H}_{fc} \parallel -\hat{\mathbf{y}}$. A large hysteresis exists between the field sweep-up ($-9 \rightarrow 9$ T, red) and sweep-down ($9 \rightarrow -9$ T, blue) curves. **b**, Same as **a** but for measurements with $\mathbf{H}_{fc} \parallel -\hat{\mathbf{x}}$. Curves measured in the new lobe direction, $\varphi = 45°$ are shown. **c**, $T$ dependence of the orthogonal susceptibility $\chi_\perp \sim M_\perp/H^2$ inferred from sweep-up (red symbols) and sweep-down (blue) curves as shown in **a** ($\mathbf{H}_{fc} \parallel -\hat{\mathbf{y}}$). Their average (black symbols) grows like an order parameter below $T_N$. **d**, Same as **c** but inferred $T$ from sweep-up (red symbols) and sweep-down (blue) curves as shown in **b** ($\mathbf{H}_{fc} \parallel -\hat{\mathbf{x}}$). In both **c** and **d**, the hysteresis amplitude decreases very rapidly below ~80 K, becoming unresolved below 30 K.

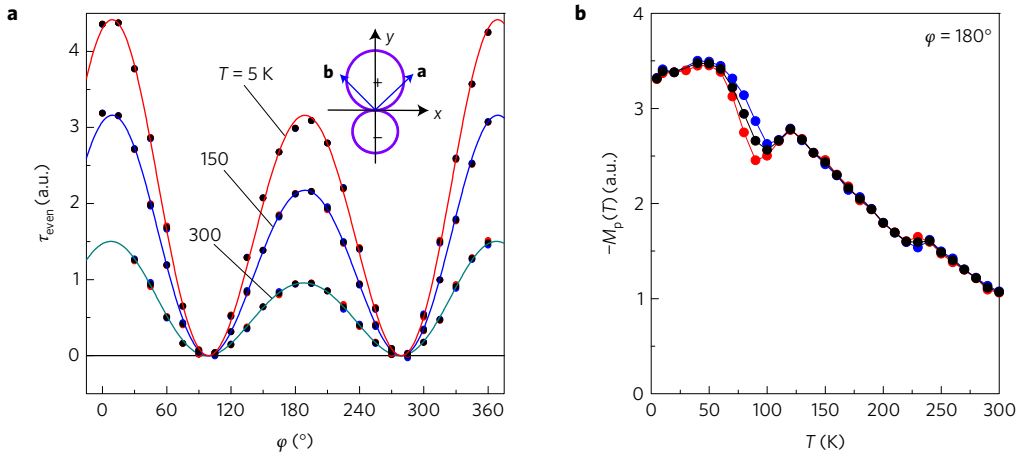


**Figure 4 | Paramagnetic magnetization. a**, Angular dependence of $H$-even component of the torque $\tau_{even}$ measured at 5, 150 and 300 K. The solid curves are fits to equation (11). Amplitude modulation caused by the parameter $\eta$ suppresses the maximum at 180° relative to that at 0° (and 360°). We estimate that $\eta = 0.17$ at 5 K, 0.18 at 150 K, and 0.22 at 300 K. The suppression is also apparent in the polar representation of the $p$-wave form in $M_p$ shown in the inset. **b**, Plots of the $T$ dependence of $M_p$ measured at $\varphi = 180°$. $M_p$ decreases monotonically between 50 K and 300 K, aside from a kink feature near $T_N$ (red and blue circles are $M_p$ measured in sweep-up and sweep-down scans; black circles are the average).

Here, $\eta$ is again the phenomenological term representing the additional order that already exists at 300 K (see below and section D of Methods). We have also explored cooling with $\mathbf{H}_{fc}$ in other directions. When cooled in say $\mathbf{H}_{fc} \parallel \mathbf{a}$, the observed $M_\perp$ versus $\varphi$ is a linear combination of the two $d$-wave patterns discussed above. Hence we infer that the two principal axes for field cooling are $\hat{\mathbf{x}} \parallel [1\bar{1}0]$ and $\hat{\mathbf{y}} \parallel [110]$ ($\hat{\mathbf{y}}$ is identified later as the axis favoured by $\eta$).

The breaking of the underlying $C_4$ lattice symmetry implies that an additional order exists above $T_N$. A first clue comes from the existence of $M_s$ above $T_N = 120$ K. Supplementary Fig. 10 shows the angular dependence of $\tau_s$ and $\tau_\perp$ at 150 K. Whereas $\tau_s$ (hence $M_s$) remains finite at 150 K and retains the same angular pattern seen at 5 K (see Supplementary Fig. 5), $\tau_\perp$ (hence $M_\perp$) vanishes completely. The differences imply that $M_s$ and $M_\perp$ are associated with very different magnetic orderings.

To investigate this additional order, we examine the paramagnetic term $M_p$, which is strictly $H$-linear, with an angular variation that remains unchanged from 5 to 300 K. Figure 4a plots $\tau_{even}(=\tau_p)$ versus $\varphi$ at $T = 5$, 150 and 300 K. The sinusoidal variation has a distorted dipolar form (inset) that fits well to the expression $(M_p/H)\cos\varphi$, where $M_p$ has the form

$$M_p(T,\varphi) = \chi_p(T)H(1+\eta\cos\varphi)\cos\varphi \qquad (11)$$

All its $T$ dependence resides in the amplitude $\chi_p(T)$ (Fig. 4b). The parameter $\eta$ (nearly independent of $T$) represents the additional order that develops along the $y$-axis, breaking the underlying $C_4$ lattice symmetry.

The symmetry breaking of handedness (chirality $\omega$) together with the activated behaviour of DWs of $M_\perp$ sharply distinguish octupolar from dipolar order. The existence of the additional order parameter $\eta$ which already exists at 300 K allows the system to assume two different $d$-wave lobe patterns of $M_\perp$. Exploring the mechanism of symmetry breaking of handedness in octupolar order—namely, what is the conjugate of the octupolar order parameter, as well as the origin of additional order $\eta$—are fruitful directions to pursue in the iridates.

## Methods

Methods, including statements of data availability and any associated accession codes and references, are available in the online version of this paper.

Received 18 April 2016; accepted 26 January 2017; published online 27 February 2017

## References


1. Pesin, D. & Balents, L. Mott physics and band topology in materials with strong spin–orbit interaction. *Nat. Phys.* **6,** 376–381 (2010).
2. Jackeli, G. & Khaliullin, G. Mott insulators in the strong spin–orbit coupling limit: from Heisenberg to a quantum compass and Kitaev models. *Phys. Rev. Lett.* **102,** 017205 (2009).
3. Witczak-Krempa, W., Chen, G., Kim, Y. B. & Balents, L. Correlated quantum phenomena in the strong spin-orbit regime. *Annu. Rev. Condens. Matter Phys.* **5,** 57–82 (2014).
4. Wan, X., Turner, A. M., Vishwanath, A. & Savrasov, S. Y. Topological semimetal and Fermi-arc surface states in the electronic structure of pyrochlore iridates. *Phys. Rev. B* **83,** 205101 (2011).
5. Turner, A. M. & Vishwanath, A. in *Topological Insulators* Vol. 6 (eds Franz, M. & Molenkamp, L.) Ch. 11, 293–324 (Elsevier, 2013).
6. Witczak-Krempa, W., Chen, G., Kim, Y. B. & Balents, L. Correlated quantum phenomena in the strong spin-orbit regime. *Annu. Rev. Condens.* **5,** 57–82 (2014).
7. Witczak-Krempa, W. & Kim, Y. B. Topological and magnetic phases of interacting electrons in the pyrochlore iridates. *Phys. Rev. B* **85,** 045124 (2012).
8. Savary, L., Moon, E.-G. & Balents, L. New type of quantum criticality in the pyrochlore iridates. *Phys. Rev. X* **4,** 041027 (2014).
9. Kim, B. J. *et al*. Novel $J_{eff} = 1/2$ Mott state induced by relativistic spin-orbit coupling in $Sr_2IrO_4$. *Phys. Rev. Lett.* **101,** 076402 (2008).
10. Kim, B. J. *et al*. Phase-sensitive observation of a spin-orbital Mott state in $Sr_2IrO_4$. *Science* **323,** 1329–1332 (2009).
11. Matsuhira, K. *et al*. Metal-insulator transition in pyrochlore iridates $Ln_2Ir_2O_7$ (Ln = Nd, Sm, and Eu). *J. Phys. Soc. Jpn* **76,** 043706 (2007).
12. Matsuhira, K., Wakeshima, M., Hinatsu, Y. & Takagi, S. Metal–insulator transitions in pyrochlore oxides $Ln_2Ir_2O_7$. *J. Phys. Soc. Jpn* **80,** 094701 (2011).
13. Ishikawa, J. J., O'Farrell, E. C. T. & Nakatsuji, S. Continuous transition between antiferromagnetic insulator and paramagnetic metal in the pyrochlore iridate $Eu_2Ir_2O_7$. *Phys. Rev. B* **85,** 245109 (2012).
14. Tafti, F. F., Ishikawa, J. J., McCollam, A., Nakatsuji, S. & Julian, S. R. Pressure-tuned insulator to metal transition in $Eu_2Ir_2O_7$. *Phys. Rev. B* **85,** 205104 (2012).
15. Sagayama, H. *et al*. Determination of long-range all-in-all-out ordering of $Ir^{4+}$ moments in a pyrochlore iridate $Eu_2Ir_2O_7$ by resonant X-ray diffraction. *Phys. Rev. B* **87,** 100403 (2013).
16. Machida, Y., Nakatsuji, S., Onoda, S., Tayama, T. & Sakakibara, T. Time-reversal symmetry breaking and spontaneous Hall effect without magnetic dipole order. *Nature* **463,** 210–213 (2010).
17. Zhao, S. *et al*. Magnetic transition, long-range order, and moment fluctuations in the pyrochlore iridate $Eu_2Ir_2O_7$. *Phys. Rev. B* **83,** 180402 (2011).
18. Yamaura, J. *et al*. Tetrahedral magnetic order and the metal–insulator transition in the pyrochlore lattice of $Cd_2Os_2O_7$. *Phys. Rev. Lett.* **108,** 247205 (2012).
19. Tomiyasu, K. *et al*. Emergence of magnetic long-range order in frustrated pyrochlore $Nd_2Ir_2O_7$ with metal–insulator transition. *J. Phys. Soc. Jpn* **81,** 034709 (2012).
20. Ueda, K. *et al*. Variation of charge dynamics in the course of metal–insulator transition for pyrochlore-type $Nd_2Ir_2O_7$. *Phys. Rev. Lett.* **109,** 136402 (2012).
21. Ueda, K. *et al*. Anomalous domain-wall conductance in pyrochlore-type $Nd_2Ir_2O_7$ on the verge of the metal–insulator transition. *Phys. Rev. B* **89,** 075127 (2014).
22. Ma, E. Y. *et al*. Mobile metallic domain walls in an all-in-all-out magnetic insulator. *Science* **350,** 538–541 (2015).
23. Glazkov, V. N. *et al*. Single-ion anisotropy in the gadolinium pyrochlores studied by electron paramagnetic resonance. *Phys. Rev. B* **72,** 020409 (2005).
24. Glazkov, V. N., Marin, C. & Sanchez, J.-P. Observation of a transverse magnetization in the ordered phases of the pyrochlore magnet $Gd_2Ti_2O_7$. *J. Phys. Condens. Matter* **18,** L429–L434 (2006).


## Acknowledgements

T.L. acknowledges a scholarship from Japan Student Services Organization. N.P.O. acknowledges the support of the US National Science Foundation (Grant DMR 1420541) and the Gordon and Betty Moore Foundations EPiQS Initiative through Grant GBMF4539. L.F. and T.H.H. were supported by DOE Office of Basic Energy Sciences, DE-SC0010526. T.H.H. thanks the KITP Graduate Fellowship Program. The research at University of Tokyo is supported by grants-in-aid (no. 16H02209) and the Program for Advancing Strategic International Networks to Accelerate the Circulation of Talented Researchers (no. R2604) from JSPS, by CREST of JST, and grant-in-aid for scientific research on Innovative Areas (Grants Nos 15H05882 and 15H05883) from MEXT.

## Author contributions

T.L., T.H.H., L.F. and N.P.O. conceived the idea behind the experiment. T.L. designed the experiment and carried out all the measurements. T.L. and N.P.O. analysed the results with important insights from T.H.H. and L.F. The manuscript was written by T.L. and N.P.O. with numerous inputs from T.H.H. and L.F. The high-quality crystal was grown by J.J.I. and S.N. The basic characterization of crystals was made by J.J.I. and S.N. All authors discussed the results and commented on the manuscript.

## Additional information

Supplementary information is available in the online version of the paper. Reprints and permissions information is available online at www.nature.com/reprints. Correspondence and requests for materials should be addressed to T.L. or N.P.O.

## Competing financial interests

The authors declare no competing financial interests.

## Methods

**Difference between the octupolar and the dipolar order.** In this section, we discuss the difference between the octupolar order and the dipolar order in detail. As mentioned in the main text, since the $Eu_2Ir_2O_7$ has inversion symmetry and the quadrupolar order vanishes, the free energy $F$ and the magnetization $\mathbf{M}$ of the system can in general be expressed as follows, viz.,

$$F = -\mathbf{M}^{\mathrm{d}} \cdot \mathbf{H} - \chi^{\mathrm{p}}_{ij} H_i H_j - \omega_{ijk} H_i H_j H_k \tag{12}$$

$$M_i = M^{\mathrm{d}}_i + \chi^{\mathrm{p}}_{ij} H_j + \omega_{ijk} H_j H_k \tag{13}$$

$$\equiv M^{\mathrm{d}}_i + M_{\mathrm{p}} + M_{\perp} \tag{14}$$

Here $\mathbf{M}^{\mathrm{d}}$ (vector) is the conventional dipolar order, $\chi_{ij}$ is the conventional paramagnetic susceptibility, and $\omega_{ijk}$ (third rank tensor) is the octupolar order. Accordingly, the magnetization can be written in terms of three terms, the dipolar term $\mathbf{M}^{\mathrm{d}}$, the paramagnetic term $M_{\mathrm{p}} = \chi^{\mathrm{p}}_{ij} H_j$, and the orthogonal magnetization term $M_{\perp} = \omega_{ijk} H_j H_k$. Whereas both $\mathbf{M}^{\mathrm{d}}$ and $\omega_{ijk}$ change sign under time reversal operation, $\chi_{ij}$ stays unchanged. In a conventional antiferromagnet (AF)/ferromagnet (FM), only the first two terms of equations (13) and (14) are finite and the octupolar order $\omega_{ijk}$ is absent. Therefore, detection of the orthogonal magnetization $M_{\perp} = \omega_{ijk} H_j H_k$ is the direct evidence for the 'hidden order' of the system.

Our torque magnetometry experiments detect magnetization perpendicular to the applied magnetic field along the $z$-axis, $M_z = M_{\mathrm{s}} + M_{\mathrm{p}} + M_{\perp}$ with $M_{\mathrm{s}} \propto H^0$ the field-independent term, $M_{\mathrm{p}} \propto H$ the paramagnetic term, and $M_{\perp} \propto H^2$ the orthogonal magnetization term.

Below, we show that the orthogonal magnetization $M_{\perp}$ detected in our experiments comes from the octupolar order $\omega_{ijk}$, and not from the contamination of the conventional dipolar order $\mathbf{M}^{\mathrm{d}}$. In the conventional AF/FM, the dipolar magnetization $\mathbf{M}^{\mathrm{d}}$ is simply represented as the sum of local dipoles $\boldsymbol{m}_i$ consisting the system, that is, $\mathbf{M}^{\mathrm{d}} = \sum_1^N \boldsymbol{m}_i$, with $N$ the total number of lattice sites. If $\mathbf{M}^{\mathrm{d}} = \sum_1^N \boldsymbol{m}_i = 0$, then no magnetization can be detected, and orthogonal magnetization $M_{\perp} = 0$ rigorously holds. More in general, if $\mathbf{M}^{\mathrm{d}} = \sum_1^N \boldsymbol{m}_i \neq 0$, then in principle $\mathbf{M}^{\mathrm{d}}$ can appear, if any, in the $M_{\mathrm{s}}$ term of our experiment, and it can even take highly nonlinear behaviour like the case of $Gd_2Ti_2O_7$, where the trivial 'transverse' magnetization $\mathbf{M}^{\mathrm{d}} = \mathbf{M}_{\mathrm{trans}}$ can appear as a consequence of distortion of the spin configuration[23,24]. However, if this were the case and $M_{\perp}$ merely came from the contamination of dipolar order $\mathbf{M}^{\mathrm{d}}$ for $Eu_2Ir_2O_7$, then the hysteretic behaviour of $M_{\mathrm{s}}$ and $M_{\perp}$ would have been the same because they would have shared the same source $\mathbf{M}^{\mathrm{d}}$. However, as evidenced in Fig. 1d in the main text, at 5 K, while $M_{\perp}$ is completely frozen, showing no hysteresis at all, $M_{\mathrm{s}}$ changes sign and manifests a large hysteresis. The angular and temperature dependences of the hysteresis curves of $M_{\mathrm{s}}$ and $M_{\perp}$ also manifest completely different behaviours, as shown in Supplementary Figs 4 and 5. Furthermore, as mentioned in the main text, while the $M_{\mathrm{s}}$ term persists above $T_N \sim 120$ K, and is related to the phenomenological $\eta$ term which is already present at 300 K, orthogonal magnetization $M_{\perp}$ emerges only below $T_N = 120$ K. These pieces of evidence sharply distinguish the different origins between $M_{\mathrm{s}}$ and $M_{\perp}$, excluding the possibility of contamination of dipolar order $\mathbf{M}^{\mathrm{d}}$ into orthogonal magnetization $M_{\perp}$. We also note that whereas $M_{\perp}$ and $M_{\mathrm{s}}$ change sign under flipping the field-cooling direction, $M_{\mathrm{p}}$ does not, so the origin of $M_{\perp}$ can easily be separated out from the paramagnetic term $M_{\mathrm{p}}$ as well.

Another way to see that the orthogonal magnetization $M_{\perp}$ cannot be explained by the contamination of conventional dipolar order $\mathbf{M}^{\mathrm{d}}$ comes from the comparison of the relevant Zeeman energy scale. We contrast the case of $Eu_2Ir_2O_7$, where orthogonal magnetization $M_{\perp}$ appears, with the case of the conventional AF $Gd_2Ti_2O_7$, where the trivial dipolar magnetization, previously called 'transverse' magnetization $\mathbf{M}^{\mathrm{d}} = \mathbf{M}_{\mathrm{trans}}$, appears due to the distortion of spin configuration via the Zeeman energy. In $Gd_2Ti_2O_7$, the relevant macroscopic exchange energy is $J_{\mathrm{eff}} \sim T_N \sim 1$ K (=0.0866 meV) (the microscopic exchange energy is much higher than this) and the magnetic moment is $\sim 7\mu_{\mathrm{B}}$ (=7.28 meV at 9 T)[25]. Therefore, under an applied magnetic field, it is easy to distort the spin configuration to induce the dipolar 'transverse' magnetization $\mathbf{M}^{\mathrm{d}} = \mathbf{M}_{\mathrm{trans}}$ normal to the applied magnetic field. Indeed, in ref. 24, $Gd_2Ti_2O_7$ shows a sharp kink $\sim 3$ T in torque data, signalling the distortion of the spin configuration. Above $\sim 3$ T, the local dipoles $\boldsymbol{m}_i$, which comprise the system, tilt towards the direction of applied magnetic field through the conventional dipolar coupling $-\mathbf{M}^{\mathrm{d}} \cdot \mathbf{H}$ to give a highly nonlinear dipolar 'transverse' magnetization $\mathbf{M}^{\mathrm{d}} = \mathbf{M}_{\mathrm{trans}} = \sum_1^N \boldsymbol{m}_i$ that cannot be decomposed into the simple polynomial form as seen in $Eu_2Ir_2O_7$ (see the data for $Gd_2Ti_2O_7$ in ref. 24 for comparison). At sufficiently high applied magnetic field, every local magnetic dipole completely aligns towards the applied magnetic field, and the 'transverse' magnetization $\mathbf{M}^{\mathrm{d}} = \mathbf{M}_{\mathrm{trans}}$ vanishes completely. By contrast, in the case of $Eu_2Ir_2O_7$, the relevant macroscopic exchange energy is $J_{\mathrm{eff}} \sim T_N \sim 120$ K (=10.4 meV) (microscopic exchange energy is much higher than this) and the magnetic moment of iridium ion $Ir^{4+}$ is $< 1.1\mu_{\mathrm{B}}$ (=1.14 meV at 9 T)[17,26,27]. The Zeeman energy induced by the magnetic field is too small to distort the spin configuration under an experimentally accessible field up to 9 T. Indeed, our torque data fit to the simple polynomial form $\tau = \alpha H + \beta H^2 + \gamma H^3$ very smoothly, showing that there is no distortion of the spin configuration. This sharply distinguishes the case of $Eu_2Ir_2O_7$, where the orthogonal magnetization $M_{\perp} = \omega_{ijk} H_j H_k$, that is, octupolar order $\omega_{ijk}$, is observed, from the case of $Gd_2Ti_2O_7$, where the trivial dipolar 'transverse' magnetization $\mathbf{M}^{\mathrm{d}} = \mathbf{M}_{\mathrm{trans}}$ is observed. See section C for more details.

**Spontaneous symmetry breaking of handedness (chirality $\omega$) in $\mathbf{M}_{\perp}$.** In this section, we discuss the spontaneous symmetry breaking of handedness (chirality $\omega$) in the orthogonal magnetization $M_{\perp}$ in detail. As shown in previous section A, the orthogonal magnetization $M_{\perp} = \omega_{ijk} H_j H_k$ is the thermodynamical manifestation of the octupolar order $\omega_{ijk}$. As shown in the main text, the measured orthogonal magnetization $M_{\perp}$ can be represented as follows, depending on the field-cooling direction:

$$M_{\perp} = \omega \chi^{y_{fc}}_{\perp} H_a H_b \quad (\pm y\text{-axis field cooling}) \tag{15}$$

$$M_{\perp} = \omega \chi^{x_{fc}}_{\perp} H_x H_y \quad (\pm x\text{-axis field cooling}) \tag{16}$$

The magnetization response is along the direction orthogonal to the plane defined by $\hat{\mathbf{a}}$ and $\hat{\mathbf{b}}$ (or equivalently, $\hat{\mathbf{x}}$ and $\hat{\mathbf{y}}$)—that is, $\mathbf{M}$ is in the $\hat{\mathbf{z}}$ direction. Accordingly, we call it $M_{\perp}$. It should now be apparent that spontaneous symmetry breaking happens. The free energy $F$ in equation (12) does not dictate whether $M_{\perp}$ is along $+\hat{\mathbf{z}}$ or along $-\hat{\mathbf{z}}$ (both are allowed). However, in response to $\mathbf{H}$ applied in the $a$–$b$ plane, the system spontaneously selects one direction. If the direction $+\hat{\mathbf{z}}$ is selected, the chirality $\omega = +1$. One cannot predict a priori whether $\mathbf{H}$ applied strictly in the $a$–$b$ plane gives rise to an $M_{\perp} \cdot \hat{\mathbf{z}} > 0$ or $M_{\perp} \cdot \hat{\mathbf{z}} < 0$. The existence of this spontaneous orthogonal magnetization is the central message of our work.

We now contrast the foregoing with a conventional AF where the 'transverse' magnetization induced by $\mathbf{H}$ seems to have engendered considerable confusion. The applied $\mathbf{H}$ couples to individual subunit moments (for example, on Mn in $MnF_2$) by the Zeeman energy $E_z$. Because the moments cant towards the direction of $\mathbf{H}$, there is no spontaneous symmetry breaking of the type discussed above. Following convention, we call the magnetization of the two sublattices $\mathbf{M}_{\mathbf{A}}$ and $\mathbf{M}_{\mathbf{B}}$ (they are nominally antiparallel). First, if $\mathbf{H} \perp (\mathbf{M}_{\mathbf{A}} - \mathbf{M}_{\mathbf{B}})$, we obtain a canting of both sublattice magnetizations towards $\mathbf{H}$, leading to a net magnetization 'transverse' to $(\mathbf{M}_{\mathbf{A}} - \mathbf{M}_{\mathbf{B}})$, namely $\mathbf{M}_{\mathrm{trans}} \perp (\mathbf{M}_{\mathbf{A}} - \mathbf{M}_{\mathbf{B}})$. This is a trivial Zeeman-driven 'transverse' magnetization whose direction is dictated by $\mathbf{H}$. On the other hand, if $\mathbf{H} \parallel (\mathbf{M}_{\mathbf{A}} - \mathbf{M}_{\mathbf{B}})$, the Zeeman response is initially weak. Increasing $\mathbf{H}$ leads to a spin-flop transition at which $\mathbf{M}_{\mathbf{A}} - \mathbf{M}_{\mathbf{B}}$ suddenly aligns perpendicular to $\mathbf{H}$. Above the spin flop, we again obtain the same 'transverse' magnetization $\mathbf{M}_{\mathrm{trans}} \perp (\mathbf{M}_{\mathbf{A}} - \mathbf{M}_{\mathbf{B}})$. In both orientations, there is no spontaneous symmetry breaking; $\mathbf{M}_{\mathrm{trans}}$ trivially aligns with $\mathbf{H}$. As discussed at length in sections A and C, in the conventional AF $Gd_2Ti_2O_7$, such 'transverse' magnetization has been previously observed (the spin configuration distorts under an applied magnetic field $\mathbf{H}$ and generates the 'transverse' magnetization, see sections A and C for details). Crucially, the suppression of this Zeeman-induced coupling in $Eu_2Ir_2O_7$ allows the octupolar response to be observed.

Finally, the observed orthogonal magnetizations $M_{\perp}$ in equations (15) and (16) take two $d$-wave patterns when $\mathbf{H}$ is rotated in the $a$–$b$ plane as shown in Fig. 2. Such $d$-wave variation versus $\varphi$ with alternating signs cannot be produced by the 'transverse' magnetization in a conventional AF.

**Difference between $\mathbf{M}_{\perp}$ and $\mathbf{M}_{\mathrm{trans}}$.** In this section, we discuss in some detail how the orthogonal magnetization $\mathbf{M}_{\perp}$ observed in this work is distinct from the 'transverse' magnetization $\mathbf{M}_{\mathrm{trans}}$ previously studied in the pyrochlore magnet $Gd_2Ti_2O_7$ (refs 23,24). Their origins and physical implications are very different. (In refs 23,24, the notation $\mathbf{M}_{\perp}$ was used for 'transverse' magnetization $\mathbf{M}_{\mathrm{trans}}$. Here we reserve $\mathbf{M}_{\perp}$ for our orthogonal magnetization and use $\mathbf{M}_{\mathrm{trans}}$ to represent the 'transverse' magnetization for clarity.)

*Review of $M_{\mathrm{trans}}$ in refs* 23,24. Following ref. 23, we write the Hamiltonian for a pyrochlore magnet $Gd_2Ti_2O_7$:

$$\hat{\mathcal{H}} = J \sum_{\langle ij \rangle} \mathbf{S}_i \cdot \mathbf{S}_j + D \sum_i (\mathbf{n}_i \cdot \mathbf{S}_i)^2 - \mathbf{H} \cdot \sum_i \mathbf{S}_i \tag{17}$$

The first term in equation (17) is the Heisenberg interaction term with $J > 0$. The sum runs over the nearest-neighbour sites. The second term is the single-ion interaction term and the third term is the Zeeman coupling term in an applied field $\mathbf{H}$. $\mathbf{S}_i$ represents the spin on site $i$. $\mathbf{n}_i$ ($i = 1$–4) are the local easy axes.

When $D>0$, the single-ion term favours alignment of the spin in the local easy plane normal to $\mathbf{n}_i$. However, the Heisenberg and Zeeman terms favour $\mathbf{S}_{\rm tet} \parallel \mathbf{H}$, where $\mathbf{S}_{tet}=\sum_i^4 \mathbf{S}_i$ is the sum of the four spins in each tetrahedron. The two conditions can be simultaneously satisfied when the applied $H$ is small, in which case $\mathbf{S}_{tet}=\mathbf{H}/2J$, so no 'transverse' magnetization $M_{\rm trans}$ appears. However, since the first constraint restricts the maximum possible value of $\mathbf{S}_{\rm tet}^{\rm max}$ to be smaller than the saturation value of $\mathbf{S}_{tet}^{sat}=4S$, the Zeeman term causes the spins to cant out of the local easy plane when $\mathbf{H}$ exceeds $\mathbf{H}_c=2J\mathbf{S}_{tet}^{max}$. Hence $\mathbf{S}_{tet}\neq\mathbf{H}/2J$, resulting in the appearance of a 'transverse' magnetization $\mathbf{M}_{\rm trans}$. With further increase in $H$, each spin fully aligns with $\mathbf{H}$ (when $H>H_{sat}$), and $\mathbf{M}_{\rm trans}$ vanishes.

We note that the direction of $\mathbf{M}_{\rm trans}$, induced by canting of the spins out of the local easy plane via Zeeman coupling to $\mathbf{H}$, is completely dictated by $\mathbf{H}$. It is not related to octupolar order, and does not involve spontaneous breaking of a discrete symmetry.

*Orthogonal magnetization* $\mathbf{M}_\perp$. Next we describe the orthogonal magnetization $\mathbf{M}_\perp$ observed in our experiments.

1. The orthogonal magnetization $\mathbf{M}_\perp$, which develops below $T_N=120$ K, is given by equations (15) and (16). We note that it involves the chirality $\omega$ multiplied by a susceptibility $\chi$—that is, $\omega\chi_\perp$. By contrast, the 'transverse' magnetization $\mathbf{M}_{\rm trans}$ is the normal component of the magnetization induced by the Zeeman term.
   A key point of the orthogonal magnetization $M_\perp$ is related to the spontaneous symmetry breaking dictated by the sign of the chirality $\omega$; namely, despite the field cooling along the $+y$-axis ($+x$-axis) and the $-y$-axis ($-x$-axis) nominally gives no difference, the sign of the order parameter (that is, chirality $\omega$) changes sign, breaking the symmetry. We emphasize that the configurations of dipoles shown in Supplementary Fig. 1 serve only as the symmetry constraint of the octupolar order the system can take, and the dipoles themselves are not our focus. In other words, equations (15) and (16) do not come from the canting of the spins; $\mathbf{M}_\perp$ is not induced by a Zeeman term.
2. A sharp distinction between $\mathbf{M}_\perp$ and $\mathbf{M}_{\rm trans}$ is shown by the hysteretic behaviour. As shown in Fig. 3c and d (main text) and in Supplementary Fig. 6, $\mathbf{M}_\perp$ does not show any hysteresis below 30 K, whereas large hysteresis is observed between 30 K and 120 K. This is very different from hysteresis caused by the motion of conventional Bloch domain walls.
3. Separation of $\mathbf{M}_\perp$ from other terms $M_{\rm s}$ and $M_{\rm p}$. The observed total magnetization $\mathbf{M}_{obs}$ is the sum of three terms, viz. $\mathbf{M}_{obs}=\mathbf{M}_{\rm s}+\mathbf{M}_{\rm p}+\mathbf{M}_\perp$. All terms are perpendicular to the applied magnetic field. The only important contribution that emerges from the octupolar magnetic order is $\mathbf{M}_\perp$. We carefully separated out each contribution. It is worth remarking that $\mathbf{M}_\perp$ does not arise from Taylor expansion of the field-independent magnetization $\mathbf{M}_{\rm s}$ or the paramagnetic term $\mathbf{M}_{\rm p}$. First, one can separate $\mathbf{M}_\perp$ from $\mathbf{M}_{\rm p}$. Whereas $\mathbf{M}_\perp$ changes sign if the direction of the field-cooling field $\mathbf{H}_{\rm fc}$ is inverted, $\mathbf{M}_{\rm p}$ does not. This shows that the two terms are distinct. Further, the $\mathbf{M}_{\rm s}$ term is easily distinguished from the $\mathbf{M}_\perp$ term by their qualitatively different hysteretic behaviour versus field, angle and temperature, as discussed in Supplementary Section 4.

**Additional order $\eta$.** In this section we discuss additional order $\eta$ and its relation to $M_{\rm s}$, $M_{\rm p}$, $M_\perp$.

1. In addition to $\mathbf{M}_\perp$ related to octupolar order, which develops below $T_N=120$ K, another order represented by $\eta$ (nearly independent of temperature) develops at least up to 300 K ($\eta=0.22$), suggesting the origin of $\eta$ is related to a higher energy scale.
2. The $\eta$ develops along the $y$-axis, breaking the underlying lattice symmetry between the $y$-axis ([110]-axis) and the $x$-axis ([$1\bar{1}0$]-axis), the two 'equivalent' axes if only lattice symmetry is considered.
3. The $\eta$ couples to each of the terms $M_{\rm s}$, $M_{\rm p}$, and $\mathbf{M}_\perp$, both below and above $T_N$.
   (a) The $M_{\rm s}$ term (as well as the $M_{\rm p}$ term) remains finite above $T_N=120$ K (see Supplementary Fig. 10), above which $\mathbf{M}_\perp$ (namely, the octupolar order) vanishes. This again implies that both $M_{\rm s}$ and $M_{\rm p}$ are unrelated to $\mathbf{M}_\perp$. Since the only order parameter which exists above $T_N=120$ K is $\eta$, we speculate $M_{\rm s}$ is intimately related to $\eta$.
   (b) The paramagnetic term $M_{\rm p}$ is perpendicular to the applied magnetic field and shows a Curie–Weiss-like temperature dependence. In general, the perpendicular paramagnetic term can arise in any anisotropic system, and itself is a trivial effect. The paramagnetic term $M_{\rm p}$ inherits the anisotropy of $\eta$, breaking the underlying lattice symmetry of the $x$- and $y$-axes.
   (c) Since $\eta$ persists above $T_N=120$ K, above which $\mathbf{M}_\perp$ vanishes, the origin of $\eta$ is different from $\mathbf{M}_\perp$. However, the fact that $\eta$ breaks underlying lattice symmetry between the $x$- and $y$-axes allows $\mathbf{M}_\perp$ to assume different $d$-wave patterns depending on whether the field-cooling direction $\mathbf{H}_{\rm fc}$ is along the $x$-axis (equation (16)) or the $y$-axis (equation (15)).
4. An unusual anisotropy coming from $\eta$ makes the absolute value at $\varphi=0^\circ$ ($+y$-axis) different from $\varphi=180^\circ$ ($-y$-axis) for $\mathbf{M}_\perp$ and $M_{\rm p}$. This is anomalous, as the $+y$-axis and the $-y$-axis should be the same except for flipping the definition of the sign of the applied magnetic field. We take account of this effect phenomenologically by adding the term $\eta\cos\varphi$.

**Data availability.** The data that support the plots within this paper and other findings of this study are available from the corresponding authors upon reasonable request.

## References


25. Narumi, Y. *et al*. High field magnetization of the pyrochlore compound $Gd_2Ti_2O_7$. *AIP Conf. Proc.* **850,** 1113–1114 (2006).
26. Disseler, S. M. *et al*. Magnetic order in the pyrochlore iridates $A_2Ir_2O_7$ ($A=$ Y, Yb). *Phys. Rev. B* **86,** 014428 (2012).
27. Shapiro, M. C. *et al*. Structure and magnetic properties of the pyrochlore iridate $Y_2Ir_2O_7$. *Phys. Rev. B* **85,** 214434 (2012).